ACS APPLIED MATERIALS & INTERFACES

Research Article

www.acsami.org

# Graphene Oxide Assisted Fluorescent Chemodosimeter for High-Performance Sensing and Bioimaging of Fluoride Ions

Changyao Wang,† Sheng Yang,† Mei Yi, Changhui Liu, Yijun Wang, Jishan Li, Yinhui Li, and Ronghua Yang*

State Key Laboratory of Chemo/Biosensing and Chemometrics, College of Chemistry and Chemical Engineering, and Collaborative Innovation Center for Chemistry and Molecular Medicine, Hunan University, Changsha 410082, China

Supporting Information

**ABSTRACT:** Fluorescent chemodosimeters for a fluoride ion ($F^-$) based on a specifically $F^-$-triggered chemical reaction are characterized by high selectivity. However, they are also subjected to intrinsic limits, such as long response time, poor stability under aqueous solution, and unpredictable cell-member penetration. To address these issues, we reported here that the self-assembly of fluorescent chemodosimeter molecules on a graphene oxide (GO) surface can solve these problems by taking advantage of the excellent chemical catalysis and nanocarrier functions of GO. As a proof of concept, a new $F^-$-specific fluorescent chemodosimeter molecule, **FC-A**, and the GO self-assembly structure of **GO/FC-A** were synthesized and characterized. Fluorescent sensing and imaging of $F^-$ with **FC-A** and **GO/FC-A** were performed. The results showed that the reaction rate constant of **GO/FC-A** for $F^-$ is about 5-fold larger than that of **FC-A**, so that the response time was shortened from 4 h to about 30 min, while for $F^-$, the response sensitivity of **GO/FC-A** was >2-fold higher than that of **FC-A**. Furthermore, **GO/FC-A** showed a better bioimaging performance for $F^-$ than **FC-A** because of the nanocarrier function of GO for cells. It is demonstrated that this GO-based strategy is feasible and general, which could help in the exploration of the development of more effective fluorescent nanodosimeters for other analytes of interest.

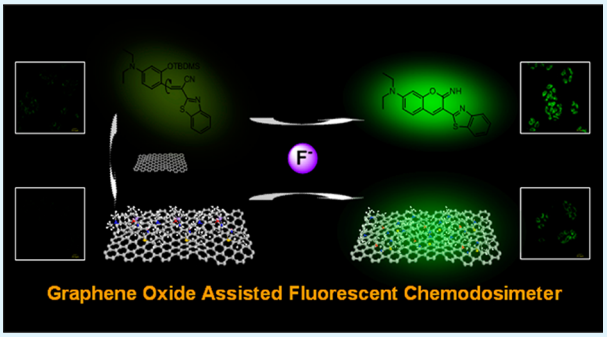


**KEYWORDS:** *graphene oxide, fluorescent chemodosimeter, fluoride ion, biosensing and bioimaging*

## INTRODUCTION

The fluoride anion ($F^-$), as the smallest anion, plays indispensable roles in a wide range of physiological processes such as the prevention of dental caries and osteoporosis treatment.[1,2] Thus, fluoride as a useful additive is frequently found in toothpaste, pharmaceutical agents, and even drinking water. However, excess intake of fluoride may cause adverse effects for human health.[3] Dental and skeletal fluorosis, neurological damages, endocrine dyscrasia, and urolithiasis are associated with high levels of $F^-$ in drinking water.[4−8] Additionally, sodium fluoride can disturb various cell-signaling processes and induce apoptosis in cells.[9,10] Taking these effects into account, the accurate determination of $F^-$ is of growing importance in both environmental and biological systems.

In comparison with conventional assay methods for $F^-$ including ion-selective electrode, colorimetry, and capillary electrophoresis,[11−13] fluorescent techniques display apparent advantages such as operational simplicity, high sensitivity, and bioimaging analysis in living cells, even in vivo.[14] Over the past decades, numerous fluorescent probes for $F^-$ have been designed by exploiting different strategies, including hydrogen-bonding interaction, Lewis acid coordination, and fluorescent chemodosimetry.[15−17] Among them, the last one appears to be more attractive because of its higher selectivity.[18] Hence, considerable efforts have been made to develop fluorescent chemodosimeters for the recognition and bioimaging of $F^-$ based on $F^-$-triggered cleavage reaction of the Si−O bond.[19−23] Unfortunately, most of them proposed so far are confronted with some drawbacks in environment and bioimaging applications. First, limited by the inevitable hydration of $F^-$ in water and low concentrations of chemodosimeters to avoid concentration quenching effects induced by self-absorption or self-quenching, tens of minutes or even hours are required to complete the detection process.[24] Second, organic fluorophores usually have innate defects, including less water solubility, unpredictable cell-member penetration, and poor photostability and chemical stability.[25] Therefore, how to address these issues and improve the sensing and bioimaging performances of $F^-$ fluorescent chemodosimeters to make them more suitable for environmental and biological systems represents a worthwhile pursuit.

To achieve the above goals, remarkable progress has been made through the introduction of a hydrophilic substrate to the probe molecule by chemical modification[26] and asking

Received: April 11, 2014
Accepted: May 17, 2014
Published: May 17, 2014

 © 2014 American Chemical Society  dx.doi.org/10.1021/am502142d | ACS Appl. Mater. Interfaces 2014, 6, 9768−9775

functional nanomaterials with unique and tunable properties for help, for example, surfactant micelles, polymers, and hydrogels.[27−29] However, reduced sensitivity by unimproved self-quenching of dyes and troublesome preparation procedures limit their pervasive application. So, there is still plenty of room for improving the performances of $F^-$ fluorescent chemodosimeters. In the view of organic chemistry, interactions of fluorescent chemodosimeters with target analytes, in essence, are organic chemical reactions. Enhancing reaction efficiencies would conceivably bring a fitness benefit for the performances of fluorescent chemodosimeters. It is a pity that, apart from a few examples of using metal-catalyzed organic reaction,[30] less attention has been paid to facilitating reaction transformations of fluorescent chemodosimeters for improving their performances, not to mention using nanomaterials. Hence, the proposal of a simple and efficient strategy with new nanomaterials for facilitating the response efficiency of a $F^-$ fluorescent chemodosimeter is of our interest.

Following this line of thought, we turn our attention to graphene oxide (GO) because its extraordinary physicochemical and structural properties have sparked extensive applications in different fields, such as biomedicine, catalysis, bioanalysis, and so forth.[31−34] As a part of our ongoing interest in carbon nanomaterial-based biosensors,[35−38] we recently reported that the assembly of a $F^-$-specific silyl-appended spiropyran dye with GO allowed rapid and sensitive colorimetric detection of $F^-$ in aqueous solution,[39] which may be because GO plays the role of catalyst in the acceleration and improvement of organic reaction.[40] In light of this work, we supposed that the sensing performance, especially transformation, of a fluorescent chemodosimeter for $F^-$ may also be forcefully improved with the help of GO. Furthermore, in the presence of GO, a $F^-$-specific fluorescent chemodosimeter would have better biocompatibility in bioimaging application because of the nanocarrier function of GO toward organic small molecules through $\pi-\pi$-stacking interaction.[41] Therefore, we herein present a novel approach, namely, a GO-assisted fluorescent chemodosimeter, to improve the sensing and bioimaging performances of fluorescent chemodosimeters for $F^-$. To verify the feasibility of our proposed approach, a new $F^-$-specific fluorescent chemodosimeter, **FC-A**, and the GO self-assembly structure of **GO/FC-A** were synthesized and characterized. As expected, the nanocomposite **GO/FC-A** displays a better response toward $F^-$ in aqueous solution than free fluorescent chemodosimeter **FC-A** and has been successfully used for the measurement of $F^-$ in water samples. Furthermore, the results of living cell imaging demonstrate that **GO/FC-A** shows a better bioimaging performance for $F^-$ than **FC-A** because of the nanocarrier function of GO.

## EXPERIMENTAL SECTION

**Materials and Apparatus.** All chemicals were obtained from commercial suppliers and used without further purification. $^1H$ and $^{13}C$ NMR spectra were recorded on a Bruker DRX-400 spectrometer operating at 400 and 100 MHz, respectively. All chemical shifts are reported in the standard $\delta$ notation of parts per million. Liquid chromatography−mass spectrometry analyses were performed using an Agilent 1100 HPLC/MSD spectrometer. Atomic force microscopy (AFM) measurements were performed using a Nanoscope Vmultimode atomic force microscope (Veeco Instruments, Plainview, NY). High-performance liquid chromatography (HPLC) analyses were performed using a LC-20A chromatograph (Shimadzu Corp., Kyoto, Japan). Energy-dispersive X-ray (EDX) analysis was carried out using a Hitachi S-4500 instrument. For Raman measurements, a confocal microprobe Raman instrument (RamLab-010; Jobin Yvon Horiba, Longjumeau, France) was used. UV−vis absorption spectra were recorded in 1-cm-path-length quartz cuvettes on a Hitachi U-4100 UV−vis spectrophotometer (Kyoto, Japan). Fluorescence emission spectra were recorded on a PTI fluorescence spectrophotometer with the excitation slit set at 2.5 nm and emission at 2.5 nm. The pH measurements were carried out on a Mettler-Toledo Delta 320 pH meter. Fluorescence images of the HeLa cells were obtained using an Olympus FV1000-MPE multiphoton laser scanning confocal microscope (Tokyo, Japan).

**Synthetic Procedure of Chemodosimeter FC-A and Nanodosimeter GO/FC-A.** Chemodosimeter **FC-A** and corresponding fluorophore **IC-B** were synthesized according to the sequences summarized in Scheme S1 of the Supporting Information (SI). GO nanosheets were synthesized according to the report of Dai and coworkers.[41] The stock solution of GO (2.0 mg/mL) was obtained by sonicating the final product for 2 h in a twice-distilled aqueous solution. The mixture solution of **FC-A** and GO was obtained by the addition of GO to the solution of **FC-A**. After stirring for about 2 h, the **GO/FC-A** nanocomposite and free **FC-A** were separated by a dialysis method, and then the product was dried under vacuum at 60 °C overnight. The structure and chemical composition of GO and **GO/FC-A** were characterized by AFM and EDX spectroscopy.

**Spectrophotometric Experiments.** Because of the poor water solubility, the stock solution of **FC-A** (0.5 mM) and **IC-B** (0.5 mM) was obtained by dissolving the material in ethanol. All stock solutions of anions were prepared from analytical-grade sodium salts and were dissolved in doubly distilled water. A 1.0 mL test solution of **FC-A** (10 $\mu$M) in a buffered ethanol solution [20 mM HEPES; $H_2O$/EtOH = 50/50 (v/v); pH 7.4] was first introduced to a quartz cell, and then 10 $\mu$L of a work solution of $F^-$ was added into the above solution. Different from **FC-A**, a test solution of **GO/FC-A** was prepared by mixing the same concentration of a **FC-A** solution with a sonicated homogeneous GO solution. The resulting solutions of chemodosimeter **FC-A** and nanodosimeter **GO/FC-A** were kept at ambient temperature for 4 h and 40 min, respectively, and then the fluorescence intensities were recorded. The fluorescence emission spectra were recorded with an excitation wavelength of 450 nm. In kinetic studies, the apparent rate constant $k'$ for the reaction of **FC-A** and **GO/FC-A** with $F^-$ was determined by fitting the fluorescence intensities to the pseudo-first-order equation[42]

$$\mathrm{Ln}[(F_{max} - F_t)/F_{max}) = -k't$$

where $F_t$ and $F_{max}$ are the fluorescence intensities at 521 nm at a time $t$ and the maximum value obtained after the reaction was complete.

The observed rate constant $k'$ contains the concentration of $F^-$ as a constant and is related to the second-order rate constant $k$ ($M^{-1}$ $s^{-1}$) by equation

$$k' = k[F^-]$$

**Real Water Sample Analysis.** The water samples were first filtered through a column (packed with an ion-exchange resin) to remove oils and other organic impurities. The fluorescence responses of the samples were compared to the calibration curve. The water samples were spiked with $5.0 \times 10^{-6}$, $1.0 \times 10^{-5}$, and $1.5 \times 10^{-5}$ M $F^-$ in recovery experiments. For comparison purposes, the fluoride levels in the same buffered samples were determined using a classical fluoride-ion-selective electrode purchased from Fisher Scientific.

**Cell Cytotoxic Assays and Imaging.** The living HeLa cells were obtained from the biomedical engineering center of Hunan University (Changsha, China) and cultured using high-glucose Dulbecco's modified Eagle's medium (DMEM; Gibco) with 1% penicillin−streptomycin (10000 U/mL, 10000 $\mu$g/mL, Invitrogen) and 10% fetal bovine serum (Gibco). The cytotoxic effects of GO, **FC-A**, and **GO/FC-A** were assessed using MTT assays. Briefly, $1.0 \times 10^4$ cells/well were seeded onto 96-well plates and allowed to grow for 48 h prior to treatment with different concentrations of GO, **FC-A**, and **GO/FC-A**. After 24 h, the medium was replaced with phosphate-buffered saline (PBS). At the end of this time, MTT was then added (final concentration 0.5 mg/mL) for 4 h at 37 °C and formazan crystals

formed through MTT metabolism by viable cells were dissolved in dimethyl sulfoxide. Optical densities were measured at 570 nm using an AC100-120 microplate reader. Immediately prior to the imaging experiments, the cells were washed with PBS, incubated with **FC-A** (5 $\mu$M) or **GO/FC-A** (10 $\mu$g/mL GO, 5 $\mu$M **FC-A**) (with 1% ethanol in the culture medium) for 4 h in the incubator at 37 °C with 5% $CO_2$, and then rinsed three times with PBS. Further, 10 $\mu$L of a 200 mM NaF solution was used to treat the cells for another 4 h and 40 min, respectively, after the addition of a new culture medium. After being washed with PBS buffer, the cells were subjected to imaging analysis using an Olympus FV1000 laser confocal microscope. Fluorescence imaging (490−520 nm) was obtained by excitation with a multiargon laser (488 nm) and analyzed by *ImageJ* software.

## RESULTS AND DISCUSSION

Our design strategy is shown in Scheme 1; a fluorescent chemodosimeter **FC-A** has been reversely designed from highly fluorescent iminocoumarin dyes **IC-B** through splitting of its lactone and then masking of the exposed phenol derivative with *tert*-butyldimethylsilyl (TBDMS). Desilylation reaction of **FC-A** by $F^-$ and subsequent intramolecular nucleophilic addition between phenolic oxygen and the nitrile group would result in the recovery of **IC-B**.[43] **FC-A** and **IC-B** were synthesized according to the sequences summarized in Scheme S1 of the SI, and then **FC-A** was simply assembled with GO by Dai's method to generate nanodosimeter **GO/FC-A** through $\pi-\pi$-stacking interaction.

**Scheme 1. Schematic Illustration of the Design of Fluorescent Chemodosimeter FC-A and GO-Based Fluorescent Nanodosimeter GO/FC-A and Their Responses to $F^-$ Ions**

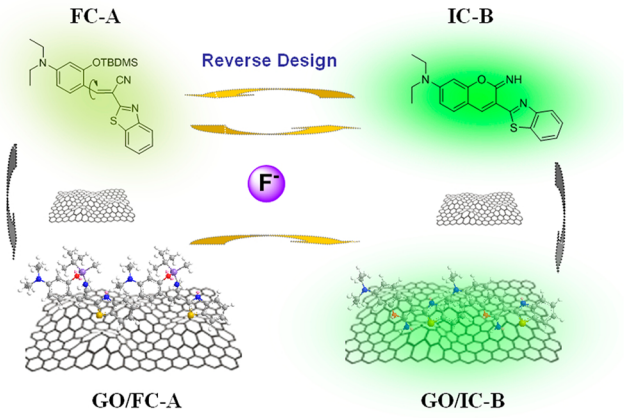


GO and **GO/FC-A** were first characterized by AFM. As shown in Figure S1A of the SI, the lateral sizes of the GO sheets were mostly lower than 200 nm, which will increase the cell uptake effciency of GO and be beneficial for bioimaging,[44] and the thickness of GO is about 1.0 nm, which is consistent with the result reported previously,[45] whereas the height of **GO/FC-A** displayed by AFM increased to 1.6 nm (Figure S1B of the SI). A comparison with the thicknesses of GO and **GO/FC-A** demonstrates that **FC-A** molecules covered the face of GO via $\pi-\pi$ stacking. The UV−vis absorbance of GO peaked at 230 nm with a shoulder at 300 nm, whereas an additional peak of **GO/FC-A** at 456 nm, the $\lambda_{max}$ of **FC-A**, clearly appeared, illustrating the interaction between GO and **FC-A** (Figure S2 of the SI). Additionally, Raman spectra of GO and **GO/FC-A** both exert a D band at 1355 $cm^{-1}$ and a G band at 1600 $cm^{-1}$, respectively, but the $I_D/I_G$ ratio of the latter (1.38) is greater than that of the former (1.25), suggesting an increment in disorder of carbon $sp^2$ hybridization probably because of the presence of **FC-A** (Figure S3 of the SI).[46] All of the above data together support the successful self-assembly of the **GO/FC-A** nanocomposite.

With **FC-A** and **GO/FC-A** both in hand, experiments on the contrast of their response performances were then explored. As exhibited in Figure 1A, the fluorescence emission spectrum of **FC-A** displays a very weak emission, peak-centered maximum at 515 nm (curve a), proving our guess that internal bond rotation results in fast nonradiative decay of the single excited state.[47] Accordingly, **IC-B** shows strong fluorescence emission with a peak maximum at 521 nm (curve b). The differences of the emission intensity between **FC-A** and **IC-B** imply the possibility of constructing a "switch-on" fluorescent sensing approach. Drastic fluorescence enhancement after the treatment of **FC-A** with $F^-$ (curve c) and HPLC analysis (Figure S4 of the SI) demonstrate the feasibility of our proposed design strategy of a chemodosimeter for $F^-$ sensing. Compared with **FC-A** and **IC-B**, respectively, **GO/FC-A** (curve a′) and **GO/IC-B** (nanocomplex of GO and **IC-B**, curve b′) both show subdued fluorescence emission spectra because GO can act collectively as a quencher for the fluorophores via energy- or electron-transfer processes.[48] However, the ratio of the emission intensity between **GO/FC-A** and **GO/IC-B** has not

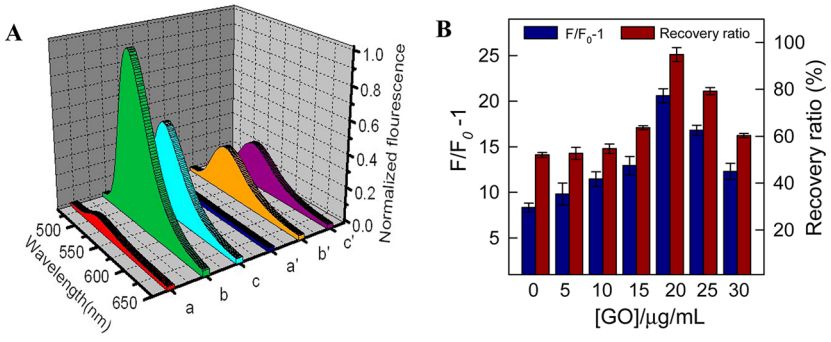


**Figure 1.** (A) Normalized fluorescence emission spectra of **FC-A** (a), **IC-B** (b), **FC-A** + $F^-$ (c), **GO/FC-A** (a′), **GO/IC-B** (b′), and **GO/FC-A** + $F^-$ (c′) in a buffer solution. [**FC-A**] = 10 $\mu$M, [**IC-B**] = 10 $\mu$M, [GO] = 20 $\mu$g/mL, and [$F^-$] = 5 mM. $\lambda_{ex}$ = 450 nm. (B) Variations of the fluorescence intensity (blue) and fluorescence recovery ratio (red) of **FC-A** + $F^-$ and **GO/FC-A** + $F^-$ versus different concentrations of GO. [**FC-A**] = 10 $\mu$M, [**IC-B**] = 10 $\mu$M, [GO] = 0−30 $\mu$g/mL, and [$F^-$] = 5 mM. $\lambda_{ex}/\lambda_{em}$ = 450 nm/521 nm. All error bars were obtained through the detection of three parallel samples.


dx.doi.org/10.1021/am502142d | ACS Appl. Mater. Interfaces 2014, 6, 9768−9775

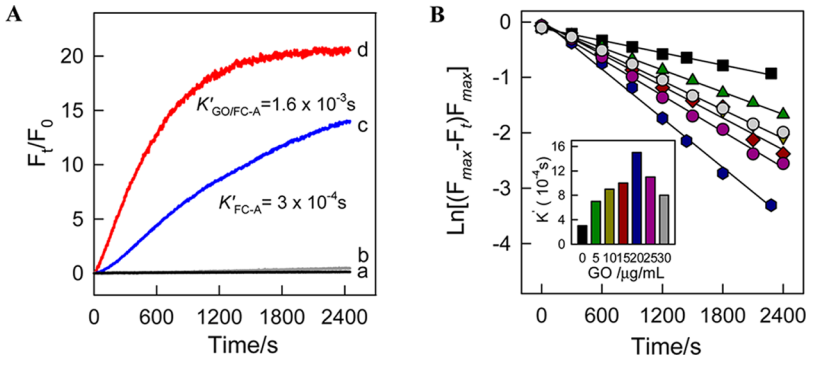


**Figure 2.** (A) Time-based fluorescence intensity changes ($F_t/F_0 - 1$) of **GO/FC-A** (a), **FC-A** (b), **FC-A** + $F^-$ (c), and **GO/FC-A** + $F^-$ (d) in a buffer solution. [**FC-A**] = 10 $\mu$M, [GO] = 20 $\mu$g/mL, and [$F^-$] = 5 mM. $\lambda_{ex}/\lambda_{em}$ = 450 nm/521 nm. (B) Effect of GO on pseudo-first-order kinetic plots of Ln[($F_{max} - F_t$)/$F_{max}$] versus time for the reaction of **GO/FC-A** with $F^-$. Inset: variations of the observed $k'$ versus concentration of GO. [**FC-A**] = 10 $\mu$M, [GO] = 0–30 $\mu$g/mL, and [$F^-$] = 5 mM. $\lambda_{ex}/\lambda_{em}$ = 450 nm/521 nm.

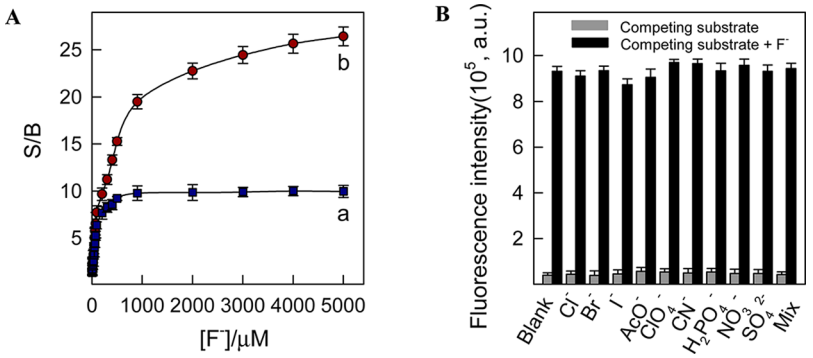


**Figure 3.** (A) S/B of **FC-A** (a) and **GO/FC-A** (b) as a function of the $F^-$ concentrations. [**FC-A**] = 10 $\mu$M, [GO] = 20 $\mu$g/mL, and [$F^-$] = 0–5 mM. $\lambda_{ex}/\lambda_{em}$ = 450 nm/521 nm. (B) Fluorescence response of **GO/FC-A** to $F^-$ (10 $\mu$M) or competing anions (5.0 mM, *x*-axis markers) and the mixture of the competing anions with $F^-$ in a buffer solution. "Mix" contains all the 10 anions. [**FC-A**] = 10 $\mu$M, and [GO] = 20 $\mu$g/mL. $\lambda_{ex}/\lambda_{em}$ = 450 nm/521 nm. All error bars were obtained through the detection of three parallel samples.

shown significant variation compared to that between **FC-A** and **IC-B** (Figure S5 of the SI). This means that **GO/FC-A** may also have the $F^-$-sensing ability with a lower background signal. As demonstrated in curve c′, the addition of $F^-$ to **GO/FC-A** also elicited a drastic fluorescence enhancement. It is noteworthy that, although the absolute fluorescence intensities of **GO/FC-A** and **GO/FC-A** + $F^-$ are lower than those of **FC-A** and **FC-A** + $F^-$, respectively, enhancement of the fluorescence intensity, $F/F_0 - 1$, of **GO/FC-A** upon the addition of $F^-$ with different concentrations of GO was bigger than that of **FC-A** (Figure 1B, blue), where $F_0$ and $F$ are the fluorescence intensities at 521 nm of **GO/FC-A** and **FC-A** with $F^-$, respectively. Superior sensitivity may be due to promotion of reaction transformation in the presence of GO, which can be represented by the higher fluorescence recovery ratio ($F_{GO/FC-A}/F_{GO/IC-B}$) of **GO/FC-A** than that ($F_{FC-A}/F_{IC-B}$) of **FC-A** (Figure 1B, red). EDX spectroscopy was employed to ensure the interactions between **GO/FC-A** and $F^-$ (Figure S6 of the SI). Compared with GO, the presence of Si, N, and S elements belonging to **FC-A** in the EDX pattern of **GO/FC-A** further indicates that noncovalent interactions of GO with **FC-A** successfully occurred. The disappearance of the Si element can be clearly seen in the EDX pattern of **GO/FC-A** + $F^-$ because $F^-$-induced cleavage of the Si–O bond weakens the interaction between the silyl functional group and GO while keeping the former far away from the latter.

Kinetic behaviors of **FC-A** and **GO/FC-A** as well as their response to $F^-$ were then studied. The fluorescence intensity change ($F_t/F_0 - 1$) of **FC-A** gradually increased with time after treatment with $F^-$ (Figure 2A, curve c). It is a pity that a relatively extended response time also was required for sufficient reaction of $F^-$ and **FC-A** (Figure S7A of the SI) similar to other reported fluorescent chemodosimeters for $F^-$ because of the aforementioned reason. However, as shown in curve d of Figure 2A and Figure S7B in the SI, the increasing trend of the fluorescence intensity change of **GO/FC-A** was obviously faster than that of **FC-A** and the response time was shortened to tens of minutes. The time-dependent processes of **GO/FC-A** response to $F^-$ with different concentrations of GO followed first-order kinetics with different observed rate constant $k'$ (Figure 2B), and the relevant observed rate constants of **GO/FC-A** with different concentrations of GO were quicker than those of **FC-A**. Meanwhile, the maximum observed rate constant of **GO/FC-A** ($k'_{GO/FC-A}$ = 1.6 × $10^{-3}$ $s^{-1}$) was about 5-fold larger than that of **FC-A** ($k'_{FC-A}$ = 3 × $10^{-4}$ $s^{-1}$). The response of **FC-A** to different concentrations of $F^-$ also followed first-order kinetics, and the plot of $k'$ versus [$F^-$] was a straight line passing through the origin (Figure S8A of the SI), which indicates that the reaction is second-order overall, with $K_{FC-A}$ = 0.323 $M^{-1}$ $s^{-1}$.[49] The second-order rate of **GO/FC-A** ($K_{GO/FC-A}$ = 3.143 $M^{-1}$ $s^{-1}$) is also bigger than that of **FC-A** (Figure S8B of the SI). It is demonstrated that GO can effectively accelerate the response of chemodosimeter **FC-A** to $F^-$. In the case of **FC-A** only (Figure 2A, curve b), a slight increase in the fluorescence intensity can be observed ascribed to hydrolysis of the Si–O bond by a buffer solution.[50]


dx.doi.org/10.1021/am502142d | ACS Appl. Mater. Interfaces 2014, 6, 9768–9775

However, no significant variation was found for **GO/FC-A** (Figure 2A, curve a). This means that a possible nanoprotective effect of GO makes **GO/FC-A** more stable than free **FC-A**.[51] This protective effect of GO can also be represented by the influence of the pH on them. As can be seen from Figure S9 of the SI, the ever-increasing fluorescence intensity of **FC-A** had been displayed in the pH range from 5.0 to 10.0, but **GO/FC-A** was less sensitive than **FC-A** in this biologically relevant pH range.

With the optimized conditions, we successively evaluated their capability for the quantitative detection of $F^-$. Figures 3A and S10 of the SI show the fluorescence responses of **FC-A** and **GO/FC-A** to different concentrations of $F^-$. After the addition of increasing concentrations of $F^-$ [$(0-9.0) \times 10^{-4}$ M] to the aqueous solution of **FC-A**, the signal-to-background ratio (S/B) elicited a dramatic enhancement trend and arrived at the maximum 9.98, where $S/B = (F - F_{buffer})/(F_0 - F_{buffer})$, in which $F$, $F_{buffer}$, and $F_0$ are fluorescence intensities at 521 nm of **FC-A** with $F^-$, buffer, and without $F^-$, respectively. However, in a comparison with **FC-A**, the dynamic response range of **GO/FC-A** to $F^-$ was enlarged to $5.0 \times 10^{-3}$ M with a corresponding S/B of 26.5, which is significantly higher than that of **FC-A**. The widened response range of **GO/FC-A** means that more $F^-$ participated in the reaction and increased the reaction efficiency.

The above experiments clearly demonstrate that **GO/FC-A** shows better response capability than free **FC-A**. We speculate the probable reason is that the improved water solubility of **FC-A** adsorbed on the GO surface, the relatively hydrophobic reaction interface provided by GO, and the intramolecular hydrogen bond via oxygen-containing functional groups of GO give rise to a decrease in the response time.[24,52] The higher sensitivity and broader response range of **GO/FC-A** than **FC-A** may be explained by the catalytic property of GO. We suppose that the presence of oxygen-carrying functionalities on the surface of GO plays a catalytic role in the activation for desilyation reaction to increase percent conversions of reaction.[53] In a word, the excellent properties of GO markedly improve the sensing performances of free **FC-A**.

On the basis of the U.S. Environmental Protection Agency, the ideal and enforceable standards for fluoride in drinking water are 0.7–1.2 ppm ($3.71 \times 10^{-5}$–$6.36 \times 10^{-5}$ M).[54] Figure S11 of the SI shows that the linear response range of **GO/FC-A** to $F^-$ covered from $2.0 \times 10^{-6}$ to $9.0 \times 10^{-5}$ M and the detection limit that is taken to be 3 times the standard derivation of a blank solution was estimated to be $\sim 3.0 \times 10^{-7}$ M, which is significantly lower than that of most published $F^-$ fluorescent probes used in drinking water.[55−58] The above experiment clearly demonstrates that **GO/FC-A** could be used as a sensitive approach for quantification of $F^-$ in aqueous solution. Selectivity experiments (Figure 3B) show that **GO/FC-A** is not only insensitive to other potentially competing anions but also selective toward $F^-$ in their presence, which is important and helpful in the validation of this nanodosimeter to meet the selectivity requirements of $F^-$ assay in environmental and biological application. Owing to the desirable sensitivity and selectivity of this approach, the practical applications of **GO/FC-A** were first evaluated by the detection of $F^-$ in river water samples (obtained from different locations of the Xiangjiang River, Changsha), and the results were compared with those given by a fluoride-ion-selective electrode method. The analytical results are shown in Table 1. All of the measurements were performed three times. The results

**Table 1. Determination of the Fluoride Ion in Water Samples and Recovery Tests Using the Proposed Method and Fluoride-Ion-Selective Electrode**

| | | $F$ (ppm) | | |
|---|---|---|---|---|
| sample | added | proposed method (mean[a] ± SD[b]) | FISE (mean[a] ± SD[b]) | recovery (%) |
| river water 1 | 0 | 0.391 ± 0.011 | 0.402 ± 0.035 | |
| river water 2 | 0 | 0.452 ± 0.006 | 0.456 ± 0.017 | |
| river water 3 | 0 | 0.367 ± 0.010 | 0.376 ± 0.025 | |
| | 0.094 | 0.469 ± 0.008 | | 102 |
| | 0.189 | 0.571 ± 0.007 | | 103 |
| | 0.377 | 0.732 ± 0.008 | | 98 |

[a]Mean value for three determinations. [b]Standard deviation.

obtained with the proposed method were in good agreement with that obtained by a fluoride-ion-selective electrode. Furthermore, the recoveries of the method were in the range of 98–103%, which evinces that the proposed method is applicable for practical $F^-$ detection.

Encouraged by the good results in vitro and successful bioimaging application of a nanoscale GO-based nanoprobe,[59−61] we then investigate whether our approach still works in a biological system. Before bioimaging experiments, the stability of **GO/FC-A** in cell culture media was first studied using a fluorescence anisotropy technique. As shown in Figure S11 of the SI, the binding of **FC-A** with GO brings about significant changes in the molecular weights and rotational diffusion rates, resulting in a bigger fluorescence anisotropy value of **GO/FC-A** than that of free **FC-A**.[62] However, fluorescence anisotropies of **FC-A** and **GO/FC-A** in cell culture media both show slight variations in comparison with a buffer solution. This means that molecules of **FC-A** display weak nonspecific protein adsorption and proteins of cell culture media cannot disturb the self-assembly of **FC-A** and **GO**. The cytotoxicities of GO, **FC-A**, and **GO/FC-A** on HeLa cells were then evaluated using a standard MTT assay (Figure S12 of the SI). After the HeLa cells were treated with GO concentrations up to 50 $\mu$g/mL for 24 h, high cell viabilities were observed (the survival rate was higher than 90% in $1.0 \times 10^4$ cells/well). Cells had no significant apoptosis when treated with low concentrations of **FC-A** (0–10 $\mu$M), but higher concentrations of **FC-A** (15–30 $\mu$M) show cytotoxicity at a certain degree, and the cell viability of **GO/FC-A** has the same tendency as that of **FC-A**. So, low concentrations of **FC-A** (5 $\mu$M) and **GO/FC-A** ($A$ = 5 $\mu$M; GO = 10 $\mu$g/mL) have been chosen for application in living cells. Then fluorescence imaging experiments were carried out in living cells on confocal laser scanning microscopy. As a control experiment, incubation of HeLa cells with only **GO/FC-A** showed no detectable fluorescence signal (Figure 4a). By contrast, the addition of sodium fluoride to HeLa cells loaded with **GO/FC-A** leads to a significant increase in the fluorescence intensity relative to the above control samples (Figure 4b). Under the same conditions, cells loaded with **FC-A** and $F^-$ displayed stronger fluorescence intensity than the ones of **GO/FC-A** treated with $F^-$ (Figure 4d), but corresponding control cells only treated with **FC-A** also show some weak fluorescence (Figure 4c). In comparison with **GO/FC-A**, a higher background fluorescence of **FC-A** significantly reduces the imaging effect and leads to an inferior S/B (Figure 4f). The above results suggest that **GO/FC-A** is

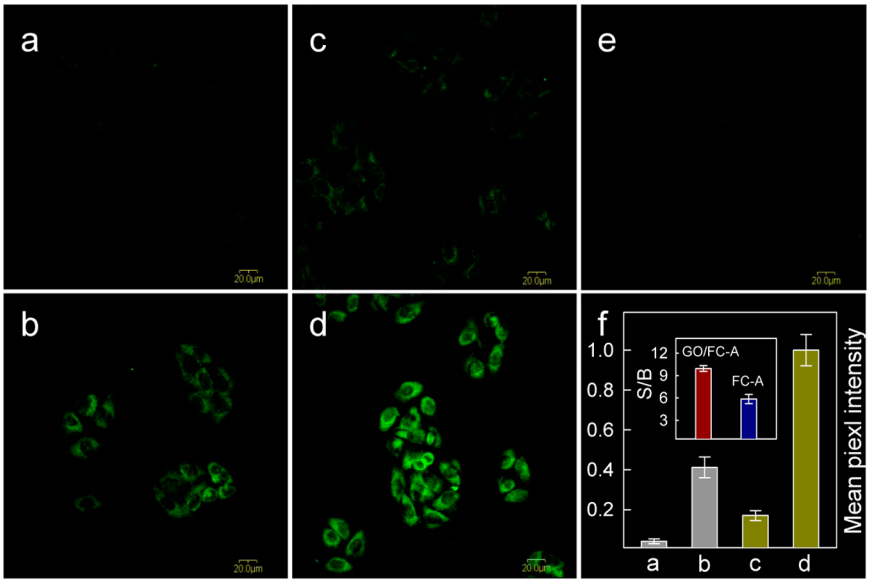


**Figure 4.** Confocal laser scanning fluorescence microscopy images of HeLa cells after incubation with **GO/FC-A** (a), **GO/FC-A** + $F^-$ (b), **FC-A** (c), and **FC-A** + $F^-$ (d) and HeLa cells only (e). The corresponding bright-field images and the overlay of fluorescence and bright-field images are shown in Figure S13 of the SI. Scale bar: 20 $\mu$m. [**FC-A**] = 5 $\mu$M, [GO] = 10 $\mu$g/mL, and [$F^-$] = 2 mM. (f) Quantification and comparison of the relative fluorescence intensity of parts a–d correspondingly. Each data point was obtained from ROIs ($n$ = 5) inside the cells.

cell-membrane-permeable and able to image fluoride ion in living cells and exhibits a superior imaging performance than free **FC-A** because of the presence of GO.

## CONCLUSION

In summary, to address the existing limitations of fluorescent chemodosimeters for $F^-$ (relatively long response time and poor bioimaging performance), a self-assembly complex of a $F^-$ fluorescent chemodosimeter on GO was prepared and their performances of fluorescent sensing and imaging were achieved by taking advantage of the chemical catalysis and nanocarrier functions of GO. This nanocomposite of a chemodosimeter displays several advantages over the free chemodosimeter molecules. First, the reaction transformation from a chemodosimeter to fluorophore was improved with the help of GO. Second, GO speeds up the reaction rate of a chemodosimeter with $F^-$ to make the response time observably shorter. Third, GO makes more $F^-$ participate in the reaction, which allowed the response range of a nanodosimeter for $F^-$ to be wider than that of a chemodosimeter for $F^-$. The well response capability of a nanodosimeter allows it to be successfully applied in the measurement of $F^-$ in water samples. Furthmore, this nanodosimeter shows a better bioimaging performance than a free chemodosimeter. To the best of our knowledge, this is the first attempt to design a fluorescent nanodosimeter by combining GO with a fluorescent chemodomister for sensing and bioimaging application. The simple design approach presented here seems to be very flexible and general, which could help in the exploration of the development of more effective fluorescent nanodosimeters for other analytes of interest. The extension of the concept of a nanocomposite of a chemodosimeter for fluorescent probe development is under progress in our laboratory.

## ASSOCIATED CONTENT

### Supporting Information

Details for the synthesis of **FC-A** and **IC-B** and characteristics of **FC-A**, **IC-B**, and fluorescent nanodosimeter **GO/FC-A**. This material is available free of charge via the Internet at http://pubs.acs.org.

## AUTHOR INFORMATION

### Corresponding Author

*E-mail: Yangrh@pku.edu.cn. Fax: +86-731-88822523.

### Author Contributions

†These authors contributed equally

### Notes

The authors declare no competing financial interest.

## ACKNOWLEDGMENTS

We are grateful for financial support from the National Natural Science Foundation of China (Grants 21135001, 21305036, 21221003, and J1103312) and the "973" National Key Basic Research Program (Grant 2011CB91100-0).

## REFERENCES

(1) Kirk, K. L. *Biochemistry of the Elemental Halogens and Inorganic Halides*; Plenum Press: New York, 1991.

(2) Kleerekoper, M. The role of fluoride in the prevention of osteoporosis. *Endocrinol. Metab. Clin. North Am.* **1998**, *27*, 441–452.

(3) Ozsvath, D. L. Fluoride and Environmental Health: A Review. *Rev. Environ. Sci. Bio/Technol.* **2009**, *8*, 59–79.

(4) Ayoob, S.; Gupta, A. K. Fluoride in Drinking Water: A Review on the Status and Stress Effects. *Crit. Rev. Environ. Sci. Technol.* **2006**, *36*, 433–487.

(5) Wang, S. X.; Wang, Z. H.; Cheng, X. T.; Li, J.; Sang, Z. P.; Zhang, X. D. Arsenic and Fluoride Exposure in Drinking Water: Children's IQ and Growth in Shanyin County, Shanxi Province, China. *Environ. Health Perspect.* **2007**, *115*, 643–647.

(6) Trivedi, M. H.; Verna, R. J.; Chinoy, N. J.; Patel, R. S.; Sathawara, N. G. Effect of High Fluoride Water on Intelligence of School Children in India. *Fluoride* **2007**, *40* (3), 178–183.

(7) Jooste, P. L.; Weight, M. J.; Kriek, J. A.; Louw, A. J. Endemic Goitre in the Absence of Iodine Deficiency in Schoolchildren of the Northern Cape Province of South Africa. *Eur. J. Clin. Nutr.* **1999**, *53*, 8−12.
(8) Singh, P. P.; Barjatiya, M. K.; Dhing, S.; Bhatnagar, R.; Kothari, S.; Dhar, V. Evidence Suggesting That High Intake of Fluoride Provokes Nephrolithiasis in Tribal Populations. *Urol. Res.* **2001**, *29*, 238−244.
(9) Arhima, M. H.; Gulati, O. P.; Sharma, S. C. The Effect of Pycnogenol on Fluoride Induced Rat Kidney Lysosomal Damage in Vitro. *Phytother. Res.* **2004**, *18*, 244−246.
(10) Matsui, M.; Morimoto, M.; Horimoto, K.; Nishimura, Y. Some Characteristics of Fluoride-Induced Cell Death in Rat Thymocytes: Cytotoxicity of Sodium Fluoride. *Toxicol. In Vitro* **2007**, *21*, 1113−1120.
(11) Kahama, R. W.; Damen, J. J. M.; Ten Cate, J. M. Enzymatic Release of Sequestered Cows' Milk Fluoride for Analysis by the Hexamethyldisiloxane Microdiffusion Method. *Analyst* **1997**, *122*, 855−858.
(12) Solé, S.; Gabbaï, F. P. A Bidentate Borane as Colorimetric Fluoride Ion Sensor. *Chem. Commun.* **2004**, *11*, 1284−1285.
(13) Breadmore, M. C.; Palmer, A. S.; Curran, M.; Macka, M.; Avdalovic, N.; Haddad, P. R. On-Column Ion-Exchange Preconcentration of Inorganic Anions in Open Tubular Capillary Electrochromatography with Elution Using Transient-Isotachophoretic Gradients. 3. Implementation and Method Development. *Anal. Chem.* **2002**, *74*, 2112−2118.
(14) Urano, Y. Novel Live Imaging Techniques of Cellular Functions and in Vivo Tumors Based on Precise Design of Small Molecule-Based 'Activatable' Fluorescence Probes. *Curr. Opin. Chem. Biol.* **2012**, *16*, 602−608.
(15) Cametti, M.; Rissanen, K. Highlights on Contemporary Recognition and Sensing of Fluoride Anion in Solution and in the Solid State. *Chem. Soc. Rev.* **2013**, *42*, 2016−2038.
(16) Wade, C. R.; Broomsgrove, A. E. J.; Aldridge, S.; Gabbaï, F. P. Fluoride Ion Complexation and Sensing Using Organoboron Compounds. *Chem. Rev.* **2010**, *110*, 3958−3984.
(17) Du, J. J.; Hu, M. M.; Fan, J. L.; Peng, X. J. Fluorescent Chemodosimeters Using "Mild" Chemical Events for the Detection of Small Anions and Cations in Biological and Environmental Media. *Chem. Soc. Rev.* **2012**, *41*, 4511−4535.
(18) Yang, Y. M.; Zhao, Q.; Feng, W.; Li, F. Y. Luminescent Chemodosimeters for Bioimaging. *Chem. Rev.* **2013**, *113*, 192−270.
(19) Kim, S. Y.; Hong, J. I. Chromogenic and Fluorescent Chemodosimeter for Detection of Fluoride in Aqueous Solution. *Org. Lett.* **2007**, *9*, 3109−3112.
(20) Bozdemir, O. A.; Sozmen, F.; Buyukcakir, O.; Guliyev, R.; Cakmak, Y.; Akkaya, E. U. Reaction-Based Sensing of Fluoride Ions Using Built-In Triggers for Intramolecular Charge Transfer and Photoinduced Electron Transfer. *Org. Lett.* **2010**, *12*, 1400−1403.
(21) Bao, Y. Y.; Liu, B.; Wang, H.; Tian, J.; Bai, R. K. A "Naked Eye" and Ratiometric Fluorescent Chemosensor for Rapid Detection of $F^-$ Based on Combination of Desilylation Reaction and Excited-State Proton Transfer. *Chem. Commun.* **2011**, *49*, 3957−3959.
(22) Zhu, B. C.; Yuan, F.; Li, R. X.; Li, Y. M.; Wei, Q.; Ma, Z. M.; Du, B.; Zhang, X. L. A Highly Selective Colorimetric and Ratiometric Fluorescent Chemodosimeter for Imaging Fluoride Ions in Living Cells. *Chem. Commun.* **2011**, *47*, 7098−7100.
(23) Kim, D.; Singha, S.; Wang, T.; Seo, E.; Lee, J. H.; Lee, S. J.; Kim, K. H.; Ahn, K. H. In Vivo Two-Photon Fluorescent Imaging of Fluoride with a Desilylation-Based Reactive Probe. *Chem. Commun.* **2012**, *48*, 10243−10245.
(24) Du, F. F.; Bao, Y. Y.; Liu, B.; Tian, J.; Li, Q. B.; Bai, R. K. POSS-Containing Red Fluorescent Nanoparticles for Rapid Detection of Aqueous Fluoride Ions. *Chem. Commun.* **2013**, *49*, 4631−4633.
(25) Lee, C.; Cheng, S.; Wang, Y.; Chen, Y.; Chen, N.; Souris, J.; Chen, C.; Mou, C.; Yang, C.; Lo, L. Near-Infrared Mesoporous Silica Nanoparticles for Optical Imaging: Characterization and In Vivo Biodistribution. *Adv. Funct. Mater.* **2009**, *19*, 215−222.
(26) Ke, B. W.; Chen, X. W.; Ni, N. T.; Cheng, Y. F.; Dai, C. F.; Dinh, H.; Wang, B. H. A Fluorescent Probe for Rapid Aqueous Fluoride Detection and Cell Imaging. *Chem. Commun.* **2013**, *48*, 2494−2496.
(27) Hu, R.; Feng, J.; Hu, D.; Wang, S.; Li, S.; Li, Y.; Yang, G. A Rapid Aqueous Fluoride Ion Sensor with Dual Output Modes. *Angew. Chem., Int. Ed.* **2010**, *49*, 4915−4918.
(28) Zheng, F. Y.; Zeng, F.; Yu, C. M.; Hou, X. F.; Wu, S. Z. A PEGylated Fluorescent Turn-On Sensor for Detecting Fluoride Ions in Totally Aqueous Media and Its Imaging in Live Cells. *Chem.—Eur. J.* **2013**, *19*, 936−942.
(29) Xiong, L.; Feng, J.; Hu, R.; Wang, S. Q.; Li, S. Y.; Li, Y.; Yang, G. Q. Sensing in 15 s for Aqueous Fluoride Anion by Water-Insoluble Fluorescent Probe Incorporating Hydrogel. *Anal. Chem.* **2013**, *85*, 4113−4119.
(30) Garner, A. L.; Song, F. L.; Koide, K. Enhancement of a Catalysis-Based Fluorometric Detection Method for Palladium through Rational Fine-Tuning of the Palladium Species. *J. Am. Chem. Soc.* **2009**, *131*, 5163−5171.
(31) Liu, Y. X.; Dong, X. C.; Chen, P. Biological and Chemical Sensors Based on Graphene Materials. *Chem. Soc. Rev.* **2012**, *41*, 2283−2307.
(32) Feng, L. Y.; Wu, L.; Qu, X. G. New Horizons for Diagnostics and Therapeutic Applications of Graphene and Graphene Oxide. *Adv. Mater.* **2013**, *25*, 168−186.
(33) Cui, L.; Song, Y. L.; Ke, G. L.; Guan, Z. C.; Zhang, H. M.; Lin, Y.; Huang, Y. S.; Zhu, Z.; Yang, C. Y. J. Graphene Oxide Protected Nucleic Acid Probes for Bioanalysis and Biomedicine. *Chem.—Eur. J.* **2013**, *19*, 10442−10451.
(34) Chung, C.; Kim, Y. K.; Shin, D.; Ryoo, S. R.; Hong, B. H.; Min, D. H. Biomedical Applications of Graphene and Graphene Oxide. *Acc. Chem. Res.* **2013**, *46*, 2211−2224.
(35) Yang, R. H.; Jin, J. Y.; Chen, Y.; Shao, N.; Kang, H. Z.; Xiao, Z. Y.; Tang, Z. W.; Wu, Y. R.; Zhu, Z.; Tan, W. H. Carbon Nanotube-Quenched Fluorescent Oligonucleotides: Probes that Fluoresce upon Hybridization. *J. Am. Chem. Soc.* **2008**, *130*, 8351−8358.
(36) Ouyang, X. Y.; Yu, R. Q.; Jin, J. Y.; Li, J. S.; Yang, R. H.; Tan, W. H.; Yuan, J. L. New Strategy for Label-Free and Time-Resolved Luminescent Assay of Protein: Conjugate $Eu^{3+}$ Complex and Aptamer-Wrapped Carbon Nanotubes. *Anal. Chem.* **2011**, *83*, 782−789.
(37) Liu, J. H.; Li, J. S.; Jiang, Y.; Yang, S.; Tan, W. H.; Yang, R. H. Combination of $\pi-\pi$ Stacking and Electrostatic Repulsion Between Carboxylic Carbon Nanoparticles and Fluorescent Oligonucleotides for Rapid and Sensitive Detection of Thrombin. *Chem. Commun.* **2011**, *47*, 11321−11323.
(38) Liu, J. H.; Wang, C. Y.; Jiang, Y.; Hu, Y. P.; Li, J. S.; Yang, S.; Li, Y. H.; Yang, R. H.; Tan, W. H.; Huang, C. Z. Graphene Signal Amplification for Sensitive and Real-Time Fluorescence Anisotropy Detection of Small Molecules. *Anal. Chem.* **2013**, *85*, 1424−1430.
(39) Li, Y. H.; Duan, Y.; Zheng, J.; Li, J. S.; Zhao, W. J.; Yang, S.; Yang, R. H. Self-Assembly of Graphene Oxide with a Silyl-Appended Spiropyran Dye for Rapid and Sensitive Colorimetric Detection of Fluoride Ions. *Anal. Chem.* **2013**, *85*, 11456−11463.
(40) Su, C. L.; Loh, K. P. Carbocatalysts: Graphene Oxide and Its Derivatives. *Acc. Chem. Res.* **2013**, *46*, 2275−2285.
(41) Liu, Z.; Robinson, J. T.; Sun, X. M.; Dai, H. J. PEGylated Nanographene Oxide for Delivery of Water-Insoluble Cancer Drugs. *J. Am. Chem. Soc.* **2008**, *130*, 10876−10877.
(42) Dale, T. J.; Rebek, J. Fluorescent Sensors for Organophosphorus Nerve Agent Mimics. *J. Am. Chem. Soc.* **2006**, *128*, 4500−4501.
(43) Kim, T. I.; Kim, H.; Choi, Y.; Kim, Y. A Fluorescent Turn-on Probe for the Detection of Alkaline Phosphatase Activity in Living Cells. *Chem. Commun.* **2011**, *47*, 9825−9827.
(44) Lu, C. H.; Zhu, C. L.; Li, J.; Liu, J. J.; Chen, X.; Yang, H.-H. Using Graphene to Protect DNA from Cleavage during Cellular Delivery. *Chem. Commun.* **2010**, *46*, 3116−3118.
(45) Ryoo, S. R.; Lee, J.; Yeo, J.; Na, H. K.; Kim, Y. K.; Jang, H.; Lee, J. H.; Han, S. W.; Lee, Y.; Kim, V. N.; Min, D. H. Quantitative and Multiplexed MicroRNA Sensing in Living Cells Based on Peptide

Nucleic Acid and Nano Graphene Oxide (PANGO). *ACS Nano* **2013**, *7*, 5882−5891.
(46) Zhang, H. L.; Wei, X. L.; Zhang, Y.; Cao, J. Y.; Liu, S. S.; He, X. P.; Chen, Q. B.; Long, Y. T.; Li, L.; Chen, G. R.; Chen, K. X. Fluorogenic Probing of Specific Recognitions between Sugar Ligands and Glycoprotein Receptors on Cancer Cells by an Economic Graphene Nanocomposite. *Adv. Mater.* **2013**, *25*, 4097−4101.
(47) Volmajer, J.; Toplak, R.; Leban, I.; Le Marechal, A. M. Synthesis of New Iminocoumarins and Their Transformations into *N*-Chloro and Hydrazono Compounds. *Tetrahedron* **2005**, *61*, 7012−7021.
(48) Kim, J. Y.; Cote, L. J.; Kim, F.; Huang, J. X. Visualizing Graphene Based Sheets by Fluorescence Quenching Microscopy. *J. Am. Chem. Soc.* **2010**, *132*, 260−267.
(49) Lim, C. S.; Masanta, G.; Kim, H. J.; Han, J. H.; Kim, H. M.; Cho, B. R. Ratiometric Detection of Mitochondrial Thiols with a Two-Photon Fluorescent Probe. *J. Am. Chem. Soc.* **2011**, *133*, 11132−11135.
(50) Kim, S. Y.; Park, J. M.; Koh, M.; Park, S. B.; Hong, J. I. Fluorescent Probe for Detection of Fluoride in Water and Bioimaging in A549 Human Lung Carcinoma Cells. *Chem. Commun.* **2009**, *45*, 4735−4737.
(51) Wang, Y.; Li, Z. H.; Hu, D. H.; Lin, C. T.; Li, J. H.; Lin, Y. H. Aptamer/Graphene Oxide Nanocomplex for in Situ Molecular Probing in Living Cells. *J. Am. Chem. Soc.* **2010**, *132*, 9274−9296.
(52) Dreyer, D. R.; Park, S.; Bielawski, C. W.; Ruoff, R. S. The Chemistry of Graphene Oxide. *Chem. Soc. Rev.* **2010**, *39*, 228−240.
(53) Su, C. L.; Acik, M.; Takai, K.; Lu, J.; Hao, S. J.; Zheng, Y.; Wu, P. P.; Bao, Q. L.; Enoki, T.; Chabal, Y. J.; Loh, K. P. Probing the Catalytic Activity of Porous Graphene Oxide and the Origin of this Behaviour. *Nat. Commun.* **2012**, *3*, 1298.
(54) Sebelius, K. HHS Recommendation for Fluoride Concentration in Drinking Water for Prevention of Dental Caries. *Fed. Regist.* **2011**, *76*, 2383−2388.
(55) Matsunaga, H.; Kanno, C.; Yamada, H.; Takahashi, Y.; Suzuki, T. M. Fluorometric Determination of Fluoride Ion by Reagent Tablets Containing 3-Hydroxy-2′-Sulfoflavone and Zirconium(IV) Ethylenediamine Tetraacetate. *Talanta* **2006**, *68*, 1000−1004.
(56) Kim, Y. M.; Gabbaï, F. P. Cationic Boranes for the Complexation of Fluoride Ions in Water below the 4 ppm Maximum Contaminant Level. *J. Am. Chem. Soc.* **2009**, *131*, 3363−3369.
(57) Rochat, S.; Severin, K. A Simple Fluorescence Assay for the Detection of Fluoride in Water at Neutral pH. *Chem. Commun.* **2011**, *47*, 4391−4393.
(58) Ashokkumar, P.; Weißhoff, H.; Kraus, W.; Rurack, K. Test-Strip-Based Fluorometric Detection of Fluoride in Aqueous Media with a BODIPY-Linked Hydrogen-Bonding Receptor. *Angew. Chem., Int. Ed.* **2014**, *53*, 2225−2229.
(59) Tan, X. H.; Chen, T.; Xiong, X. L.; Mao, Y.; Zhu, G. Z.; Yasun, E.; Li, C. M.; Zhu, Z.; Tan, W. H. Semiquantification of ATP in Live Cells Using Nonspecific Desorption of DNA from Graphene Oxide as the Internal Reference. *Anal. Chem.* **2012**, *84*, 8622−8627.
(60) Wang, Y.; Li, Z. H.; Weber, T. J.; Hu, D. H.; Lin, C. T.; Li, J. H.; Lin, Y. H. In Situ Live Cell Sensing of Multiple Nucleotides Exploiting DNA/RNA Aptamers and Graphene Oxide Nanosheets. *Anal. Chem.* **2013**, *85*, 6775−6782.
(61) Feng, B. Y.; Guo, L. J.; Wang, L. H.; Li, F.; Lu, J. X.; Gao, J. M.; Fan, C. H.; Huang, Q. A Graphene Oxide-Based Fluorescent Biosensor for the Analysis of Peptide−Receptor Interactions and Imaging in Somatostatin Receptor Subtype 2 Overexpressed Tumor Cells. *Anal. Chem.* **2013**, *85*, 7732−7737.
(62) Schröder, G. F.; Alexiev, U.; Grubmüller, H. Simulation of Fluorescence Anisotropy Experiments: Probing Protein Dynamics. *Biophys. J.* **2005**, *89*, 3757−3770.